Available online at www.sciencedirect.com
ScienceDirect
International Journal of Heat and Mass Transfer 49 (2006) 4325–4339
International Journal of HEAT and MASS TRANSFER
www.elsevier.com/locate/ijhmt

Effect of ceramic supports on microwave processing of porous food samples

Tanmay Basak [1], K. Aparna, A. Meenakshi, A.R. Balakrishnan *

Department of Chemical Engineering, Indian Institute of Technology Madras, Chennai 600 036, India

Received 6 January 2006; received in revised form 4 May 2006

Abstract

A theoretical analysis has been carried out to study efficient microwave heating of porous dielectrics. The heating effects are analyzed for two types of porous material: beef-air (b/a) and beef-oil (b/o) with and without ceramic supports (Al_2O_3 and SiC). Three test cases for porosities (ϕ) 0.3, 0.45 and 0.6 are considered. The maxima in average power corresponding to resonances occur at various sample thicknesses for all porous materials with and without supports and two dominant resonance modes R_1 and R_2 are considered where the average power at R_1 is larger than that at R_2. It is interesting to observe that average power absorption is enhanced for samples (b/a and b/o) in presence of Al_2O_3 support whereas the average power is smaller with SiC support. From the analysis on spatial distribution of electric field, power and temperature, it is seen that runaway heating is observed at the face which is not attached with support for b/a samples, and the intensity of thermal runaway increases with porosity whereas lower thermal runaway is observed for b/o samples at all porosity values. An efficient heating strategy has been investigated for various distributions of microwave incidences. It is observed that one side incidence may correspond to the largest heating rates whereas distributed sources may correspond to smaller thermal runaway for both beef-air (b/a) and beef-oil (b/o) samples.

Keywords: Microwave; Heating; Ceramic supports; Porous dielectric

1. Introduction

Electromagnetic radiations in the frequency range 300 MHz–300 GHz are known as microwaves and the typical wave lengths of microwaves are within few mm to 30 cm. Microwaves propagate through material and the accompanying transport process results in dissipation of electric energy into heat, which led to the term 'volumetric heat generation'. During microwave heating, the material dielectric loss which is a function of frequency of microwaves, is responsible to convert electric energy to heat. Dielectric response of various materials plays an important role to carry out efficient material processing and a significant amount of earlier research was devoted to understand the physics on microwave assisted transport and heating characteristics.

A detailed analysis on modeling of microwave heating has been carried out by Ayappa et al. [1,2] and their investigations were based on heating of 1D slabs and 2D cylinders. They carried out detailed theoretical analyses on coupled microwave and heat transport for pure and multilayered slabs typically used in the food industry. The localized or non-uniform heating in samples occur due to volumetric heating effects, and considerable studies were devoted to analyses of maxima in power or 'resonances' due to microwave propagation [3,4]. The heating effects during resonances are considerably greater for specific sample dimensions and the suitable relationships on occurrence of resonance with sample size were established [3,4]. Microwave heating and transport models were further applied for thawing and heating of multiphase systems in

* Corresponding author. Fax: +91 44 2257 0509.
E-mail addresses: tanmay@iitm.ac.in (T. Basak), arbala@iitm.ac.in (A.R. Balakrishnan).
[1] Fax: +91 44 2257 0509.

0017-9310/$ - see front matter © 2006 Elsevier Ltd. All rights reserved.
doi:10.1016/j.ijheatmasstransfer.2006.05.012

Nomenclature

$A_{x,l}$	amplitude of stationary wave for lth layer, V m^{-1}
Bi	Biot number (–)
c_p	specific heat capacity, J kg^{-1} K^{-1}
c	velocity of light, m s^{-1}
E_x	electric field intensity, V m^{-1}
f	frequency, Hz
h	heat transfer coefficient, W m^{-2} K^{-1}
H_y	magnetic field intensity, A m^{-1}
k	thermal conductivity, W m^{-1} K^{-1}
k	propagation constant
L	half-slab thickness, m
L_s	sample thickness, m
q	microwave source term, W m^{-3}
Q	dimensionless microwave source term
t	time, s
T	temperature, K
u	dimensionless field component
v	dimensionless real field component
w	dimensionless imaginary field component
z	distance, m
z'	dimensionless distance

Greek symbols

γ	dimensionless propagation constant
ϵ_0	free space permittivity, Farad m^{-1}
θ	dimensionless temperature
κ'	relative dielectric constant
κ''	relative dielectric loss
κ^*	relative complex dielectric properties
λ_m	wavelength in the medium, m
ρ	density, kg m^{-3}
ϕ	porosity (–)
τ	dimensionless time
$\delta_{x,l}$	phase difference in stationary wave for lth layer
ω	angular frequency, Rad s^{-1}

Subscripts

c	continuous phase
d	dispersed phase
eff	effective property
l	layer number

Superscripts

t	transmitted wave
r	reflected wave

recent investigations [5–9] and greater rates in material processing are observed due to resonances. These extensive investigations [1–9] are limited to enhanced heating effects solely due to materials. Recently, Basak and Priya [10,11] investigated the heating of water (high dielectric loss) and oil (low dielectric loss) on ceramic (Al_2O_3 and SiC) and metallic supports. In their work, the optimal heating effects with suitable support assemblies were analyzed. Common to all these studies was the study of the heating effect for pure substances in the absence of porous medium.

Current work focuses on the application of microwave heating for typical food systems. The food material may be realistically characterized as porous substances and the dielectric response of the porous substance would be non-trivial due to the effective dielectric properties of solid matrix and the fluid occupying the void space. A few earlier studies on microwave heating of porous systems were carried out for several applications such as drying of porous materials [12–14], heat and mass transfer for two phase porous materials [15] and convective drying processes [16]. Chen et al. [12] has carried out theoretical analysis on microwave heating patterns on batch fluidized bed drying of porous material. Their studies are based on three wave patterns (uniform, sinusoidal and rectangular) and the drying time is a strong function of the patterns. Ratanadecho et al. [13] carried out detailed theoretical and experimental analyses of capillary porous materials. Their analyses show that variation in particle size and initial moisture content influences the degree of penetration and rate of microwave power absorbed within the sample. Their analysis is based on strong coupling between the heating model and electromagnetic model with effective dielectric properties of the porous bed. Later Wu et al. [14] carried out theoretical analysis on conjugate heat and mass transfer on microwave freeze drying. Although their model is based on detailed analysis on heat and mass transport for drying within particles, the microwave energy is weakly coupled within the porous material. Heat and mass transfer models were also developed by Dincov et al. [15] and Salagnac et al. [16]; however the distribution of microwave power absorption within the porous bed due to effective dielectric response was absent in these analyses [14–16]. Except for the preliminary studies by Ratanadecho et al. [13], a detailed analysis which involves microwave propagation and interference of waves within the porous bed and heating effects as function of porosity is yet to appear in the literature.

The present work is an attempt to study the heating effects of typical food substances (porous beef) with or without support in the presence of microwaves. The analysis involves two typical porous bodies such as beef-air (b/a) and beef-oil (b/o) where air or oil is assumed to be the fluid

medium of the porous body. The dielectric response is modeled using effective dielectric properties for various porosity values. The efficient heating strategy corresponding to 'resonances' or maxima in microwave power has been studied for various porosity regimes. The resonances will be quite complex for a porous material–ceramic composite and as a first attempt an analysis on the resonances has been carried out for material–ceramic composite systems to study this effect on efficient heating strategies. The role of traveling waves within the porous body and ceramic supports on the heating rates are analyzed. The efficient heating mechanism characterized by 'maxima in temperature rise with minimal thermal runaway effects' has been illustrated for both beef-air (b/a) and beef-oil (b/o) with various porosity regimes and distributed microwave sources.

2. Theory

2.1. Theory of microwave radiation in porous dielectrics with ceramic supports

The porous dielectric–ceramic assembly is modeled as a one dimensional slab. The wave propagation due to uniform electric field E_x is given by Maxwell's equation

$$\frac{d^2E_x}{dz^2} + k^2E_x = 0 \tag{1}$$

where E_x lies in the x–y plane and varies only in the direction of propagation, z-axis (Fig. 1). Here, $k = \frac{\omega}{c}\sqrt{\kappa' + i\kappa''}$ is the propagation constant which depends on the dielectric constant, κ' and the dielectric loss, κ'', $\omega = 2\pi f$, where f is the frequency of the electromagnetic wave and c is the velocity of light. In a n multilayered sample, the equation

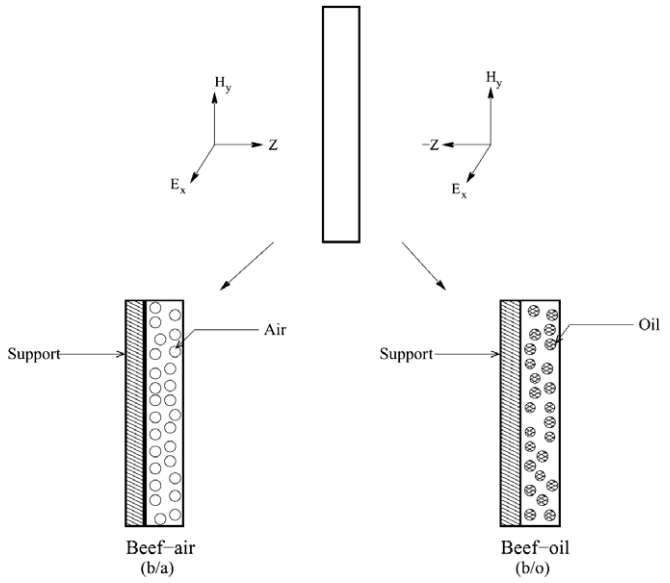

Fig. 1. Schematic illustration of a porous dielectric beef sample exposed to a plane electromagnetic wave. Two cases of porous dielectrics are considered: beef-air (b/a) and beef-oil (b/o).

for wave propagation due to electric field for the lth layer obtained from Eq. (1) is

$$\frac{d^2E_{x,l}}{dz^2} + k_l^2E_{x,l} = 0 \tag{2}$$

where $z_{l-1} \leqslant z \leqslant z_l$ and $l = 1, \ldots, n$. Assuming each layer has constant dielectric properties, the general solution to Eq. (2) represented as a linear combination of transmitted and reflected waves propagating in opposite directions is

$$\begin{aligned} E_{x,1} &= E_{t,1}e^{ik_1z} + E_{r,1}e^{-ik_1z} && \text{Air layer} \\ E_{x,l} &= E_{t,l}e^{ik_lz} + E_{r,l}e^{-ik_lz} && \text{Porous media and support} \\ & && l = 2, \ldots, n-1 \\ E_{x,n} &= E_{t,n}e^{ik_nz} + E_{r,n}e^{-ik_nz} && \text{Air layer,} \end{aligned} \tag{3}$$

where $E_{t,l}$ and $E_{r,l}$ are the coefficients due to transmission and reflection, respectively. The boundary conditions at the interface are

$$\left.\begin{aligned} E_{x,l-1} &= E_{x,l} \\ \frac{dE_{x,l-1}}{dz} &= \frac{dE_{x,l}}{dz} \end{aligned}\right\} \begin{aligned} &l = 2, \ldots, n \\ &z = z_1, z_2, \ldots, z_{n-1} \end{aligned} \tag{4}$$

Here $z_1, z_2, \ldots, z_{n-1}$ denote the boundaries between interfaces as seen in Fig. 1.

The interface conditions (Eq. (4)) and the general solutions (Eq. (3)), are used to obtain the coefficients, $E_{t,l}$ and $E_{r,l}$ by solving the set of algebraic equations:

$$\left.\begin{aligned} &E_{t,l}e^{ik_lz_l} + E_{r,l}e^{-ik_lz_l} - E_{t,l+1}e^{ik_{l+1}z_l} \\ &\quad -E_{r,l+1}e^{-ik_{l+1}z_l} = 0 \\ &k_lE_{t,l}e^{ik_lz_l} - k_lE_{r,l}e^{-ik_lz_l} - k_{l+1}E_{t,l+1}e^{ik_{l+1}z_l} \\ &\quad +k_{l+1}E_{r,l+1}e^{-ik_{l+1}z_l} = 0 \end{aligned}\right\} l = 1, \ldots, n-1 \tag{5}$$

As the incident field intensities from the left and right are known, i.e. $E_{t,l} = E_L$ and $E_{r,n} = E_R$, Eq. (5) are solved for the remaining $2n-2$ coefficients using MATLAB [7,8,10,11]. For the lth layer, the transmitted and reflected waves are

$$\begin{aligned} E^t_{x,l} &= E_{t,l}e^{ik_lz} = A^t_{x,l}e^{i\delta^t_{x,l}} \\ E^r_{x,l} &= E_{r,l}e^{-ik_lz} = A^r_{x,l}e^{i\delta^r_{x,l}} \end{aligned} \tag{6}$$

where corresponding amplitudes are given by

$$\begin{aligned} A^t_{x,l} &= \sqrt{E^t_{x,l}E^{t\,*}_{x,l}} \\ A^r_{x,l} &= \sqrt{E^r_{x,l}E^{r\,*}_{x,l}} \end{aligned} \tag{7}$$

and the phase states are given by

$$\begin{aligned} \delta^t_{x,l} &= \tan^{-1}\left[\frac{\mathrm{Im}(E^t_{x,l})}{\mathrm{Re}(E^t_{x,l})}\right] \\ \delta^r_{x,l} &= \tan^{-1}\left[\frac{\mathrm{Im}(E^r_{x,l})}{\mathrm{Re}(E^r_{x,l})}\right] \end{aligned} \tag{8}$$

where the superscript, '*' in Eq. (7) denotes the complex conjugate. For a stationary wave in the lth layer, the amplitude is given by

$$A_{x,l} = \sqrt{E_{x,l}E^*_{x,l}} \tag{9}$$

and the difference in phase angle is given by

$$\delta_{x,l} = \delta^{\mathrm{t}}_{x,l} - \delta^{\mathrm{r}}_{x,l} \tag{10}$$

where the quantities $E_{x,l}$ and $E^*_{x,l}$ in Eq. (9) are evaluated using Eqs. (3) and (6). At the resonance, the difference in phase angle is zero, i.e., $\delta_{x,l} = 0$.

The absorbed power in the lth layer, obtained from Poynting vector theorem is

$$q_l(z) = \frac{1}{2}\omega\epsilon_0\kappa''_{\mathrm{eff}}(\phi)E_{x,l}(z)E^*_{x,l}(z) \tag{11}$$

Here ϵ_0 is the free space permittivity, ϕ is the porosity and κ''_{eff} is the effective dielectric loss where,

$$\kappa^*_{\mathrm{eff}}(\phi) = \kappa'_{\mathrm{eff}}(\phi) + \mathrm{i}\kappa''_{\mathrm{eff}}(\phi) \tag{12}$$

and for a porous medium, the effective dielectric properties κ^*_{eff} can be obtained from Fricke's complex conductivity model [17]

$$\kappa^*_{\mathrm{eff}} = \frac{\kappa^*_{\mathrm{c}}[\kappa^*_{\mathrm{d}}(1+2\phi) + 2\kappa^*_{\mathrm{c}}(1-\phi)]}{\kappa^*_{\mathrm{d}}(1-\phi) + \kappa^*_{\mathrm{c}}(2+\phi)} \tag{13}$$

Here κ^*_{c} and κ^*_{d} are the relative complex dielectric properties of the continuous (beef) and dispersed (air/oil) phases, respectively. The dispersed media or the void space is assumed to be spherical. The average power obtained by integrating the power across the slab is

$$\bar{q} = \frac{1}{2L}\int_{-L}^{+L} q_l(z)\,\mathrm{d}z \approx \frac{1}{2L}\sum_{z=0}^{2L} q_l(z) \tag{14}$$

Here $-L$ and L denote the left and right faces of the slab, respectively and $q_l(z)$ denotes the power as a function of z, where z may be measured from the left edge of the slab or sample. Note that, $2L$ is the thickness of the entire slab consisting of sample and supports and L_{s} is the thickness of the sample and L' is the thickness of the support such that $2L = L_{\mathrm{s}} + L'$. The average power for a sample of thickness L_{s} is

$$q_{\mathrm{av}} = \frac{1}{n}\sum_{i=1}^{n} q_l(z_i), \quad \text{for } 0 \leqslant z_i \leqslant L_{\mathrm{s}} \tag{15}$$

2.2. Modeling of microwave heating and solution strategy

The energy balance equation for heating of a porous dielectric by microwave radiation is

$$\rho c_p\frac{\partial T}{\partial t} = k\frac{\partial^2 T}{\partial z^2} + q(z) \tag{16}$$

where ρ, the effective density, c_p, the effective specific heat and k, the effective thermal conductivity are

$$\rho = (1-\phi)\rho_{\mathrm{c}} + \phi\rho_{\mathrm{d}} \tag{17}$$

$$c_p = (1-\phi)c_{p_{\mathrm{c}}} + \phi c_{p_{\mathrm{d}}} \tag{18}$$

and

$$k = (1-\phi)k_{\mathrm{c}} + \phi k_{\mathrm{d}} \tag{19}$$

The volumetric heat source, in Eq. (16), $q(z)$ is defined in Eq. (11). In a n multilayered sample, the energy balance equation for the lth layer obtained from Eq. (16) is

$$(\rho c_p)_l\frac{\partial T_l}{\partial t} = k_l\frac{\partial^2 T_l}{\partial z^2} + q_l(z) \quad l = 1,\ldots,n \tag{20}$$

The boundary conditions are

$$k_1\frac{\partial T_1}{\partial z} = h(T_1 - T_\infty) \quad z = z_1 \tag{21}$$

and

$$-k_{n-1}\frac{\partial T_{n-1}}{\partial z} = h(T_{n-1} - T_\infty) \quad z = z_{n-1} \tag{22}$$

The interface conditions between material–ceramic are

$$\left.\begin{aligned} T_l &= T_{l+1} \\ k_l\frac{\partial T_l}{\partial z} &= k_{l+1}\frac{\partial T_{l+1}}{\partial z} \end{aligned}\right\} \quad \begin{aligned} l &= 2,3,\ldots,n-2 \\ z &= z_2, z_3, \ldots, z_{n-2} \end{aligned} \tag{23}$$

The wave propagation equation for a particular medium (ceramic/material) is given in Eq. (2). As microwave power, $q_l(z)$ is a function of electric field as seen in Eq. (11) and hence a functional representation of electric field is necessary to solve the energy balance equation (Eq. (20)). The evaluation of functional form of electric field is difficult for a multilayered sample, and therefore, the energy balance and wave equations (Eqs. (20) and (2)) are solved numerically as discussed below.

Using the dimensionless variables,

$$u = \frac{E_x}{E_0} \quad \text{and} \quad \frac{\mathrm{d}}{\mathrm{d}z'} \equiv 2L\frac{\mathrm{d}}{\mathrm{d}z}$$

Eq. (1) reduces to

$$\frac{\mathrm{d}^2 u}{\mathrm{d}z'^2} + \gamma^2 u = 0 \tag{24}$$

where u is the electric field intensity, $\gamma = \frac{2L\omega}{c}\sqrt{\kappa' + \mathrm{i}\kappa''}$ is the propagation constant and $2L$ is the thickness of the slab. Substituting the complex field variable $u = v + \mathrm{i}w$ into Eq. (24) and equating the real and imaginary components, we get

$$\frac{\mathrm{d}^2 v}{\mathrm{d}z'^2} + \chi_1 v - \chi_2 w = 0 \tag{25}$$

and

$$\frac{\mathrm{d}^2 w}{\mathrm{d}z'^2} + \chi_2 v + \chi_1 w = 0 \tag{26}$$

with $\chi_1 = \frac{4L^2\omega^2}{c^2}\kappa'$ and $\chi_2 = \frac{4L^2\omega^2}{c^2}\kappa''$. The boundary conditions for the real and imaginary components are [1],

$$\left.\begin{aligned}\frac{dv}{dz'}-\frac{2\omega L}{c}w&=\frac{4\omega L}{c}\sin\left(\frac{\omega L}{c}\right)\\ \frac{dw}{dz'}+\frac{2\omega L}{c}v&=\frac{4\omega L}{c}\cos(\frac{\omega L}{c})\end{aligned}\right\}\quad \text{at } z'=0 \tag{27}$$

and

$$\left.\begin{aligned}\frac{dv}{dz'}+\frac{2\omega L}{c}w&=-\frac{E_R}{E_L}\frac{4\omega L}{c}\sin\left(\frac{\omega L}{c}\right)\\ \frac{dw}{dz'}-\frac{2\omega L}{c}v&=-\frac{E_R}{E_L}\frac{4\omega L}{c}\cos\left(\frac{\omega L}{c}\right)\end{aligned}\right\}\quad \text{at } z'=1. \tag{28}$$

The dimensionless form of the energy balance equation in the presence of microwaves (Eq. (20)) is written as

$$(\overline{\rho c_p})_l\frac{\partial\theta_l}{\partial\tau}=\bar{k}_l\frac{\partial^2\theta_l}{\partial z'^2}+Q_l(z') \tag{29}$$

where

$$\theta_l=\frac{T_l-T_\infty}{T_0},\quad (\overline{\rho c_p})_l=\frac{(\rho c_p)_l}{\rho_0 c_{p_0}}\quad\text{and}\quad \bar{k}_l=\frac{k_l}{k_0}$$

The expression for the microwave power term in Eq. (29) is

$$Q_l(z')=\frac{2L^2\omega\epsilon_0\kappa''_{\text{eff}}(\phi)E_0^2}{k_0T_0}(v^2+w^2) \tag{30}$$

The boundary conditions in dimensionless form, Eqs. (21) and (22) are

$$\frac{\partial\theta_1}{\partial z'}-Bi_1\theta_1=0,\quad z'=0 \tag{31}$$

and

$$\frac{\partial\theta_{n-1}}{\partial z'}+Bi_{n-1}\theta_{n-1}=0,\quad z'=1 \tag{32}$$

The initial condition used in the analysis is

$$\theta(\tau=0)=\frac{T_0-T_\infty}{T_0},\quad \text{for } 0\leqslant z'\leqslant 1 \tag{33}$$

The dielectric properties are given in Table 1. Note that dielectric properties correspond to a microwave frequency of 2450 MHz. The porous dielectric may be represented by either beef-air or beef-oil with various porosities (see Fig. 1). Typical values of porosities 0.3, 0.45 and 0.6 are considered for the computation. The microwave incidence may be distributed via one source or both the sources at the sides as seen in Fig. 1. In all cases, the sample is exposed to the total microwave radiation intensity of 3 W cm^{-2}. The heat transfer coefficient at the outer surfaces is maintained at 2 W m^{-2} K^{-1}. The temperature of the sample and support is 300 K at $t=0$ s. The thickness of the sample varies between 0.1 and 5 cm and a support thickness of 0.2 cm has been assumed for all cases. It may be noted that Al_2O_3 is a transparent medium and SiC absorbs microwaves significantly [18]. A smaller thickness of support was assumed and the influence of various thicknesses of support on microwave heating of materials may not be important for the current work.

Table 1
Thermal and dielectric properties for water, oil, raw beef, Al_2O_3 and SiC [10,11,18]

Material property	Water	Oil	Raw beef	Al_2O_3	SiC
Heat capacity, C_p (J kg^{-1} K^{-1})	4190	2000	2510	1046	3300
Thermal conductivity, k (W m^{-1} K^{-1})	0.609	0.168	0.491	26	40
Density, ρ (kg m^{-3})	1000	900	1070	3750	3100
Dielectric constant, κ' (2450 MHz)	78.1	2.8	43	10.8	26.66
Dielectric loss, κ'' (2450 MHz)	10.44	0.15	15	0.1566	27.99

The energy balance equation and the electric field equations with the appropriate boundary conditions are solved using Galerkin finite element method. The interface conditions for energy balance and electric field equations due to multiple phases are automatically satisfied via an interface element common to the two phases. At the interface node, the field variables and fluxes are continuous as discussed by Reddy [19] and Ayappa et al. [1]. To discretize the time domain, the Crank–Nicholson method is used, and the non-linear residual equations are solved using the Newton Raphson Method [7,8]. Due to the lack of a good initial guess to begin the Newton scheme, a small time step $\Delta t=1\times10^{-4}$ s was used in the first step. Unless specified otherwise $\Delta t=0.1$ s was used for subsequent steps and typically 25–50 quadratic elements were used. It was found that the maximum difference for the values of the unknowns at the nodes was less than 1% when the values were compared for 25 and 50 elements. Similarly the maximum difference was less than 1% when the results were compared for $\Delta t=0.05$ and 0.1 s.

3. Results and discussion

3.1. Microwave power and temperature distributions for beef-air samples: one side incidence

A preliminary analysis on the role of ceramic supports has been carried out by examining the average power vs sample thickness diagram. The average power vs sample thickness diagram is important to further study material processing at greater heating rates which correspond to maxima in average power. The maxima in average power generally occurs at specific sample thicknesses for various materials. The maxima in average power, often termed as resonances and the two consecutive resonances may be referred to as R_1 and R_2 modes. The significant resonances occur at two consecutive R_1 and R_2 modes. The resonances (R_1 and R_2) are due to constructive interferences between transmitted and reflected waves and the amplitudes of transmitted and reflected waves are generally larger for smaller sample dimensions corresponding to the R_1 mode. Hence, the average power at R_1 mode is generally greater that at R_2 mode irrespective of the materials. Fig. 2(a)–(d) illustrate the average power vs sample thickness for samples without any support, with Alumina support on

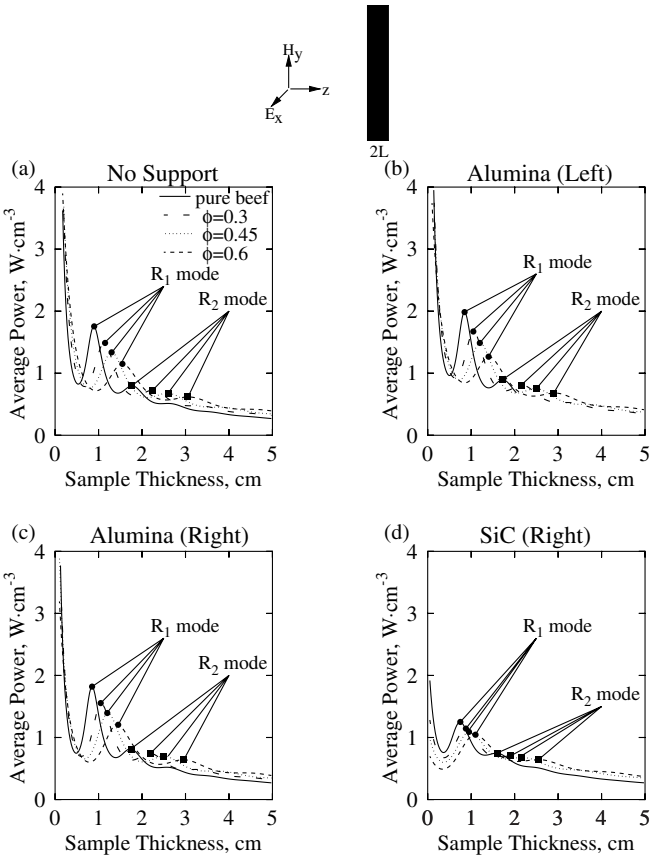

Fig. 2. Average power (W cm^{-3}) vs sample thickness (cm) for beef-air (b/a) samples with (a) no support, (b) Alumina support at the left face (c) Alumina support at the right face and (d) SiC support at the right face for pure beef and porous beef with porosities $\phi = 0.3$, 0.45 and 0.6 exposed to microwaves at one face. The symbol, ●, denotes R_1 mode and the symbol, ■, denotes R_2 mode of resonances. Higher average power is achieved with pure beef than with porous beef at R_1 mode. The sample with Alumina support at the left face exhibits larger power for pure and porous beefs at R_1 mode.

the left face, with Alumina support on the right face and with SiC support on the right face respectively. During one side incidence, the average power for a sample without any support exhibits maxima at $L_s = 0.5\lambda_m$ and λ_m during R_1 and R_2 modes, respectively [3,4]. Note that the wavelengths (λ_m) for the pure beef sample is 1.84 cm whereas the wavelengths for the beef samples with $\phi = 0.3$, 0.45 and 0.6 are 2.33, 2.70 and 3.22 cm, respectively.

It is observed from Fig. 2(a) that pure beef corresponds to greater average power than that with porous beef for all porosity values at a specific resonance mode (R_1 or R_2) without any support. It is also observed that the average power for all samples with various porosities is greater during R_1 mode. In addition, the sample thickness corresponding to R_1 and R_2 modes is found to increase as porosity increases as seen in Fig. 2(a). A similar pattern of average power with porosities is observed for microwave heating of samples with Alumina and SiC supports and the support may play a significant role on microwave heating as seen in Fig. 2(a)–(d). Fig. 2(b) shows that the average power with Alumina support at the left face enhances significantly the average power for the beef sample during R_1 mode. It may be noted that the average power is 1.75 W cm^{-3} for pure beef without any support whereas the average power is 1.98 W cm^{-3} with the Alumina support at the left face, 1.82 W cm^{-3} with Alumina support at the right face and 1.25 W cm^{-3} with SiC support. It is also observed that for all the three porosities, beef sample with Alumina support at the left side corresponds to the largest average power and the sample with SiC support corresponds to the smallest average power for both R_1 and R_2 modes.

An efficient use of supports depends on factors such as faster thermal processing, porosity of the beef sample and controlled or uniform thermal processing. The interesting features as seen in Fig. 2(a)–(d) for various cases thus provide the stimulus for determining the role of supports on efficient heating of beef samples using microwaves. A detailed analysis of microwave power characteristics and electric field distributions at various resonance modes would be useful to understand the interference of waves and the critical role of the specific ceramic support on food/material processing.

Fig. 3 shows the amplitude of the electric fields, power and temperature distributions for porous beef samples of porosities 0.3, 0.45 and 0.6 without support during R_1 mode. For all these cases, the sample thickness (L_s) corresponding to R_1 mode are 1.15, 1.3 and 1.55 cm for $\phi = 0.3$, 0.45 and 0.6, respectively. It is observed that the amplitude of the transmitted wave is a decreasing function of distance whereas the amplitude of the reflected wave is an increasing function within the sample for all porosity ranges.

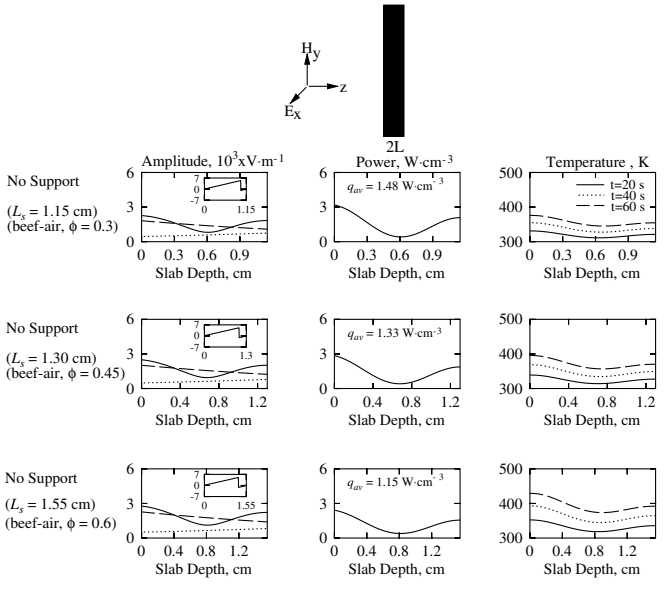

Fig. 3. Amplitudes of electric field ($A_{x,l}, A^t_{x,l}, A^r_{x,l}$), power distributions and temperature profiles for beef-air (b/a) samples without any support for porosities, $\phi = 0.3$, 0.45 and 0.6 exposed to microwaves from the left face during R_1 mode. (— —) Transmitted wave; (···) reflected wave; (——) stationary wave. The inset shows phase difference ($\delta_{x,l}$) vs z. Average power decreases with increase in porosity whereas the maxima in temperature increases with porosity.

Although the distribution of amplitudes of both the transmitted and reflected waves are found to be greater for beef sample with $\phi = 0.6$, the sample with $\phi = 0.3$ exhibits the larger spatial distribution of power due to greater dielectric loss (κ''). Therefore, the average power (q_{av}) is 1.48, 1.33 and 1.15 W cm^{-3} for $\phi = 0.3$, 0.45 and 0.6, respectively. Note that, $\kappa'' = 9.13$, 6.73 and 4.61 for $\phi = 0.3$, 0.45 and 0.6, respectively.

The insets illustrate the distribution of phase difference between the traveling waves within the sample, and a constructive interference or spatial resonance is indicated by zero phase difference. It is observed that two resonances in stationary electric field and microwave power occur at the faces of the sample. Due to greater dielectric loss, the intensity of spatial resonance is greater for sample with $\phi = 0.3$. The temperature distributions are illustrated for $t = 20$, 40 and 60 s. The temperature distributions qualitatively follow the power distributions and the two maxima in temperature occur at the faces of the samples at all times. It is interesting to note that, the sample with $\phi = 0.6$, which corresponds to smallest average power, exhibits greatest spatial temperature distribution due to smaller effective heat capacity. The specific heat capacities are 2104.67, 1902 and 1699 J kg^{-1} K^{-1} for $\phi = 0.3$, 0.45 and 0.6, respectively. At 60 s, the left face of the sample with $\phi = 0.45$ and 0.6 reaches around 400–430 K and as a result, runaway heating may occur for samples with higher porosity.

Fig. 4 illustrates the spatial distributions of amplitudes of electric fields, power and temperature for the beef samples attached with Alumina support at the left face. It is

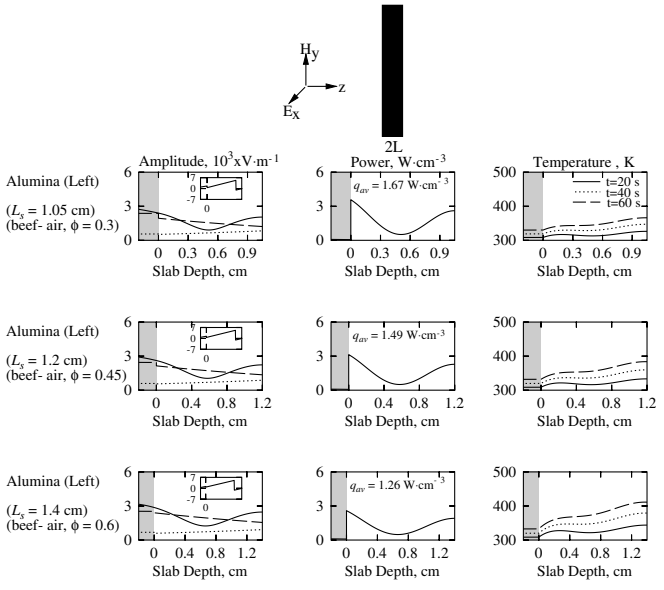

Fig. 4. Amplitudes of electric field ($A_{x,l}, A^{t}_{x,l}, A^{r}_{x,l}$), power distributions and temperature profiles for beef-air (b/a) samples with Alumina support at the left face for porosities, $\phi = 0.3$, 0.45 and 0.6 during R_1 mode. The ceramic support thickness = 0.2 cm. (— —) Transmitted wave; (···) reflected wave; (——) stationary wave. The shaded regime denotes the ceramic support. The inset shows phase difference ($\delta_{x,l}$) vs z. A sharp increase in temperature at the unexposed face is observed specially for $\phi = 0.6$.

observed that the two maxima or resonances in stationary field and power occur at the faces of the sample, as in the case without supports in Fig. 3. It is interesting to observe that there is a significant jump in amplitude of the transmitted wave within the Alumina support, especially for $\phi = 0.3$ and 0.45. As in the case without supports, the amplitudes of the traveling and stationary waves within the sample are slightly larger for $\phi = 0.6$. In addition, the Alumina support seems to enhance further the amplitudes of the waves within the sample and therefore the larger spatial power distributions are observed for samples with specific porosities. It may be noted that, the average power, $q_{av} = 1.67$, 1.49 and 1.26 W cm^{-3} for $\phi = 0.3$, 0.45 and 0.6, respectively with the Alumina support on the left face whereas $q_{av} = 1.48$, 1.33 and 1.15 W cm^{-3} for the case without support with similar porosities. The processing thickness of the sample (L_s) corresponding to R_1 mode is smaller in the presence of Alumina support at the left face and $L_s = 1.05$, 1.2 and 1.4 cm for $\phi = 0.3$, 0.45 and 0.6, respectively. It is interesting to note that, although the amplitudes of the traveling waves are quite high within Alumina support, the spatial absorption of power within Alumina is very small due to very low dielectric loss $\kappa'' = 0.1566$. Therefore Alumina supports can be used without additional power consumption.

The temperature distributions are shown for $t = 20$, 40 and 60 s. The temperature profile does not follow qualitatively the power distribution due to the presence of Alumina support. It is observed that the temperature at the unexposed face is larger than that at the exposed face. Due to greater thermal conductivity of Alumina, the temperature distributions within the support are almost flat and due to almost insulated boundary conditions ($h = 2$ W m^{-2} K^{-1}), the temperature on the unexposed face is larger. In addition, the greater heating rate at the unexposed face due to the support is more pronounced for greater porosity ($\phi = 0.6$). It is observed that the unexposed face reaches 366 K for $\phi = 0.3$, 383 K for $\phi = 0.45$ and 411 K for $\phi = 0.6$ at 60 s. It is observed that the localized runaway heating does occur at the unexposed face within the sample in the presence of support, however, the presence of Alumina support may reduce the maxima in temperature at the runaway regime. The exposed face of the sample with $\phi = 0.6$ reaches 428 K during 60 s without any support, as seen earlier in Fig. 3.

Fig. 5 illustrates the amplitude, power and temperature distributions for porous beef attached with Alumina support at the right side. Here too, two maxima in power occur at the two faces of the sample and the processing lengths (L_s) for specific porosities are almost identical with the previous case where the Alumina support is attached to the left face of the sample. It is observed that, the amplitudes of the traveling and stationary waves within the Alumina support at the right face of the sample are smaller than that within Alumina support attached at the exposed face of the sample for specific porosities (Figs. 4 and 5). It is further observed that the spatial power absorption within the

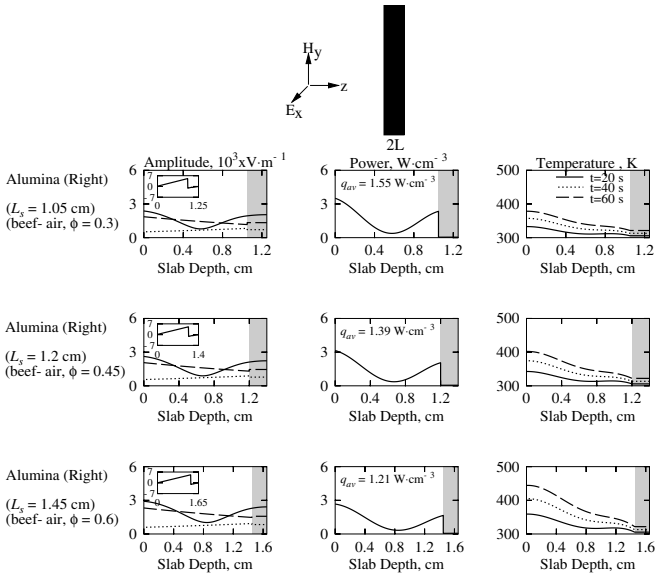

Fig. 5. Amplitudes of electric field $(A_{x,l}, A^{t}_{x,l}, A^{r}_{x,l})$, power distributions and temperature profiles for beef-air (b/a) samples with Alumina support at the right face for porosities, $\phi = 0.3$, 0.45 and 0.6 during R_1 mode. The ceramic support thickness = 0.2 cm. (— —) Transmitted wave; (···) reflected wave; (——) stationary wave. The shaded regime denotes the ceramic support. The inset shows phase difference $(\delta_{x,l})$ vs z. A sharp increase in temperature at the exposed face is observed specially for $\phi =$ 0.6.

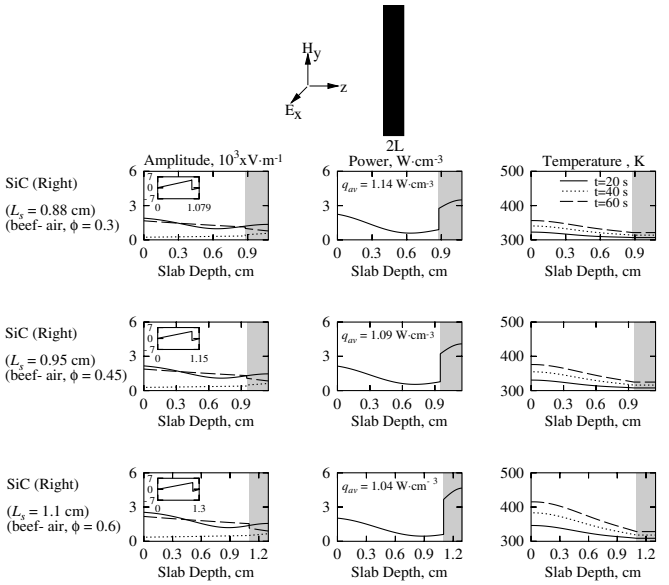

Fig. 6. Amplitudes of electric field $(A_{x,l}, A^{t}_{x,l}, A^{r}_{x,l})$, power distributions and temperature profiles for beef-air (b/a) samples with SiC support at the right face for porosities, $\phi = 0.3$, 0.45 and 0.6 during R_1 mode. The ceramic support thickness = 0.2 cm. (— —) Transmitted wave; (···) reflected wave; (——) stationary wave. The shaded regime denotes the ceramic support. The inset shows phase difference $(\delta_{x,l})$ vs z. The power absorption is smaller than that with Alumina support and with no support. A sharp increase in temperature at the exposed face is observed particularly for $\phi = 0.6$.

sample is smaller than that in the samples with support attached to the left face. However, the average power within the samples with Alumina support either on the left or right face for specific porosities is still higher than that without support. Therefore, the Alumina support either at the left or right face of the sample enhances the power within the sample and are qualitatively similar.

The temperature distribution within the sample illustrates that the maximum temperature occurs at the exposed face which is in contrast to the case where the support was on the left face (where maxima in temperature was found in the unexposed face of the beef layer). The unexposed face is found to be at very low temperature for all porosity values due to smaller power absorption within the Alumina support attached to the right face. At 60 s, it is observed that the maxima in temperatures that occur at the exposed face are 378, 402 and 444 K for $\phi = 0.3$, 0.45 and 0.6, respectively. Although Alumina support on the right face still enhances microwave power and heating rate, the runaway heating at the exposed face is greater than that without any support specially for samples with high porosity. Therefore, Alumina support attached to the unexposed face may not be suitable for efficient thermal processing.

The amplitude, power and temperature distributions are shown for porous beef attached to SiC support on the right face in Fig. 6. The sample thickness in this case is $L_s = 0.88$, 0.95 and 1.1 cm for $\phi = 0.3$, 0.45 and 0.6, respectively. The inset shows the variation of phase angle with slab depth showing zero phase difference signifying a constructive interference. Similar to earlier cases, the amplitudes of the transmitted and reflected waves increase with increase in porosity. It is interesting to note that the amplitude of the reflected wave within the sample is smaller due to the presence of SiC support and therefore, the strength of the stationary wave within the sample is considerably reduced. In addition, the smaller power within the sample may be due to greater power absorption within SiC support as SiC support corresponds to greater dielectric loss. As a consequence, the average power absorbed within the sample is lower compared to the other two cases with and without support. The average powers are 1.14, 1.09 and 1.04 W cm^{-3} for $\phi = 0.3$, 0.45 and 0.6, respectively. As in the earlier case, the maximum temperature is found to occur at the exposed face and the temperature decreases monotonically with the distance within the sample. Due to high thermal conductivity, the temperature profile is found to be uniform within SiC support. The temperature within the sample varies within 321–357 K for $\phi = 0.3$, 324–377 K for $\phi = 0.45$ and 328–418 K for $\phi = 0.6$ at 60 s. Due to lower effective heat capacities, the sample with $\phi = 0.6$ would exhibit runaway heating effect near the exposed face. The maximum temperature for $\phi = 0.6$ is 418 K. Similar to the case where Alumina support was attached to the right side, a larger temperature is reached for the case of porous beef attached to SiC support on the right side, in contrast to the situation with Alumina support attached to the left side.

Fig. 7(a)–(d) show temperature difference (ΔT_b) vs time for porous beef (b/a) without support, with Alumina sup-

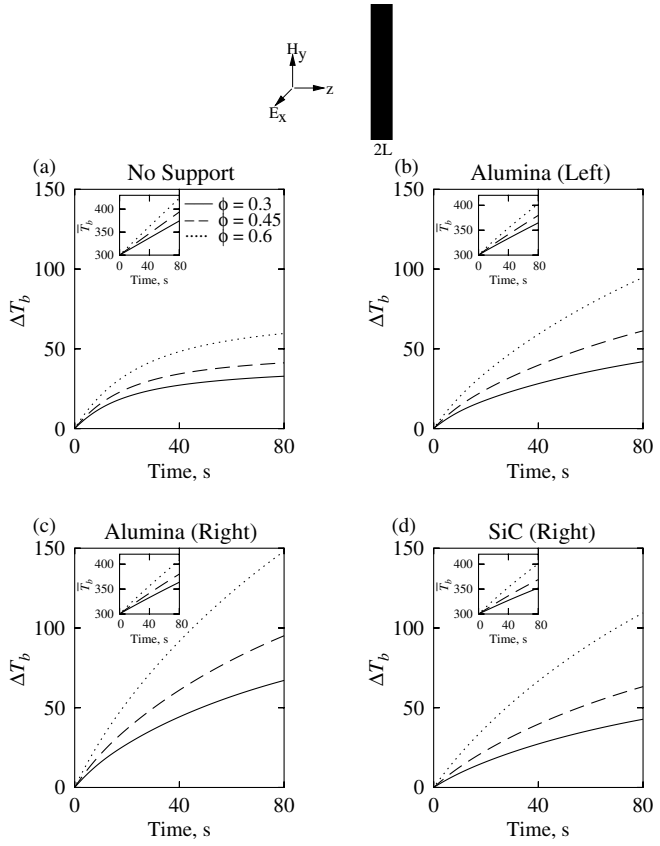

Fig. 7. The temperature difference, ΔT_b (K) vs time (s) for porous beef-air samples ($\phi = 0.3$, 0.45 and 0.6) exposed to microwaves at one face during R_1 mode for (a) no support, (b) Alumina support at the left face, (c) Alumina support at the right face and (d) SiC support at the right face. The inset shows average temperature, $\overline{T}_b$ (K) vs time (s). Larger thermal runaway is observed for higher porosity. The samples with Alumina and SiC supports at the right face show larger temperature difference or thermal runaway specially for $\phi = 0.6$.

port at left and right sides and SiC support at the right side for the three porosities mentioned earlier. It may be noted that, ΔT_b is defined as the difference between the maximum and minimum temperatures within the sample. It can be seen that temperature difference increases with increase in porosity for all cases (Fig. 7(a)–(d)). It is observed that, the largest temperature difference is found in the case of beef with Alumina support attached on the right side. In this case, the temperature difference (ΔT_b) is around 148 K for $\phi = 0.6$, 95 K for $\phi = 0.45$ and 67 K for $\phi = 0.3$ at 80 s.

The inset shows the average temperature ($\overline{T}_b$) vs time plot where the slope of the plot indicates the heating rate which is directly proportional to the microwave power absorbed. It is observed that the average temperature distribution has larger slopes for higher porosities. The average temperature vs time curve is steep for $\phi = 0.6$ for Alumina and SiC supports on the right side (Fig. 7(c) and (d)). The average temperatures for $\phi = 0.6$ at 80 s are 424, 403, 407.8 and 400.7 K for porous sample without any support, with Alumina support at the left face, with Alumina support at the right face, with SiC support at the right face, respectively. Although the average heating rate is greater for Alumina support at the left face, the greater temperature differences for supports attached at the right face is due to the steep gradient in the temperature especially for larger porosities. For small porosities ($\phi \approx 0.3$), the supports either attached at the left or right side does not alter significantly the temperature difference. The runaway situation as seen from greater ΔT_b values would occur for larger porosities. It is observed that the lower temperature differences for all porosity values occur for samples without support. The support influences the heating pattern significantly. Based on the above, the Alumina support at the left face may be recommended for optimal heating of the porous beef (b/a) sample at all porosities.

3.2. Microwave power and temperature distributions for beef-oil samples: one side incidence

Fig. 8(a)–(d) show the average power vs sample thickness with no support, Alumina support on left side,

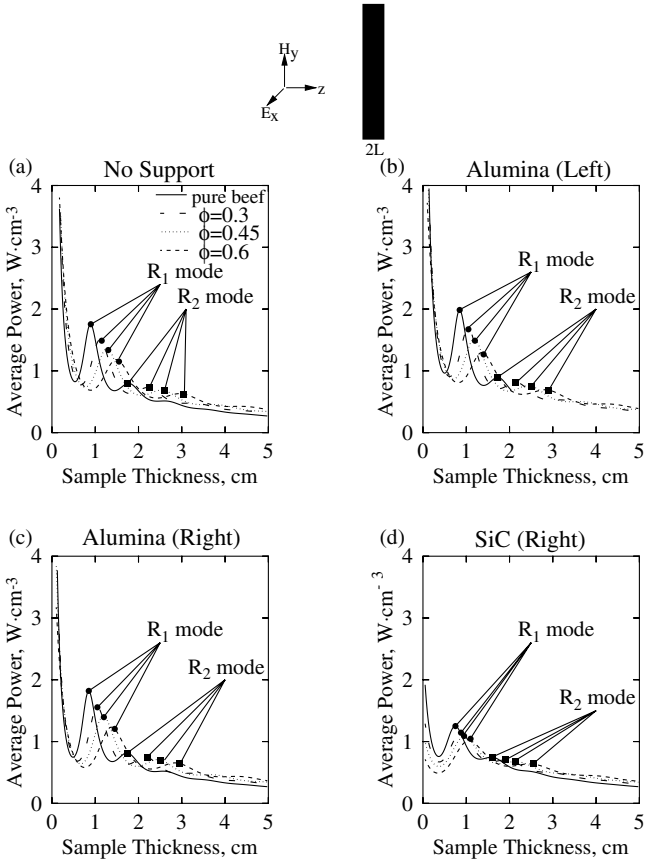

Fig. 8. Average power (W cm^{-3}) vs sample thickness (cm) for beef-oil (b/o) samples with (a) no support, (b) Alumina support at the left face, (c) Alumina support at the right face and (d) SiC support at the right face for pure beef and porous beef with porosities $\phi = 0.3$, 0.45 and 0.6 exposed to microwaves at one face. The symbol, ●, denotes R_1 mode and the symbol, ■, denotes R_2 mode of resonances. Higher average power is achieved with pure beef than with porous beef at R_1 mode. The sample with Alumina support at the left face exhibits larger power for pure and porous beefs at R_1 mode.

Alumina support on right side and SiC support on right side, respectively. The distributions are qualitatively similar to that for the beef-air case. As in Fig. 2, pure beef with zero porosity exhibits the highest average power, and as porosity increases the sample thickness corresponding to R_1 mode increases. The average power for pure beef at R_1 mode are 1.75, 1.98, 1.82 and 1.25 W cm^{-3} with no support, Alumina support at left side, Alumina support at right side and SiC support at right side, respectively. Higher power absorption occurs in presence of Alumina support at left side whereas lower power absorption is found with SiC support on right side.

The spatial distributions of power and temperature for porous beef samples of porosities 0.3, 0.45 and 0.6 without support (figures not shown) have been analyzed. Similar to beef-air sample, the sample thickness (L_s) for $\phi = 0.6$ is greater than that for smaller porosities. The spatial distributions of amplitudes of the traveling and stationary waves are qualitatively similar to those of beef-air sample for all porosity values and similar to beef-air case the average power for $\phi = 0.3$ is the largest due to high dielectric loss. The temperature profile follows qualitatively the power profile and the temperatures at 60 s vary within 339–351 K, 338–351 K and 336–352 K for $\phi = 0.3$, 0.45 and 0.6, respectively. Unlike the beef-air sample, the runaway situation at the left face of the sample does not occur due to the higher values of effective heat capacity for various porosities of beef-oil samples.

Fig. 9 shows the spatial distribution of amplitude, power and temperature for porous beef with Alumina support attached to the left face. Similar to the beef-air case, there are two power maxima at the two sides of the porous body and the average power is greater than that with no support for all porosity values. The average power is 1.69, 1.51 and 1.30 W cm^{-3} for $\phi = 0.3$, 0.45 and 0.6, respectively, while it was 1.51, 1.36 and 1.18 W cm^{-3} for the no support case. At 60 s, the temperature varies between 326–345 K, 325–345 K and 322–345 K for $\phi = 0.3$, 0.45 and 0.6, respectively. Similar to the no support situation, there is no thermal runaway situation at the outer faces of the sample. In contrast, beef-air sample with Alumina support exhibits thermal runaway at the unexposed face especially with $\phi = 0.6$ (Fig. 4). The heating procedure for samples with Alumina and SiC supports attached at the right side (figures are not shown) were also analyzed. The overall heating rate is found to be higher with Alumina support attached at right side whereas the heating rates are smaller with SiC support. The power absorbed with Alumina support are 1.57, 1.41 and 1.23 W cm^{-3} whereas with SiC support the power is 1.13, 1.08 and 1.01 W cm^{-3} for the three porosities respectively. The variation of temperature is between 315 and 360 K with Alumina support at the right face whereas with SiC support the temperature varies between 319 and 344 K at 60 s for $\phi = 0.6$. As in the case with Alumina support at the left face, there may be no significant thermal runaway at the outer faces of the sample.

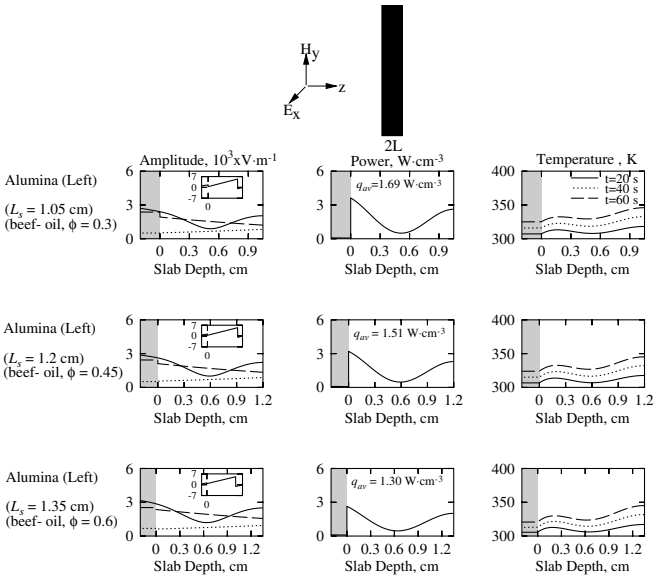

Fig. 9. Amplitudes of electric field ($A_{x,l}, A^{t}_{x,l}, A^{r}_{x,l}$), power distributions and temperature profiles for beef-oil (b/o) samples with Alumina support at the left face for porosities, $\phi = 0.3$, 0.45 and 0.6 during R_1 mode. The ceramic support thickness = 0.2 cm. (— —) Transmitted wave; (···) reflected wave; (——) stationary wave. The shaded regime denotes the ceramic support. The inset shows phase difference ($\delta_{x,l}$) vs z. A larger temperature is observed at the unexposed face specially for $\phi = 0.6$. However, the temperature rise is smaller than that with beef-air (b/a) samples as seen in Fig. 4.

Fig. 10 shows the temperature difference (ΔT_b) and average temperature ($\overline{T}_b$) vs time curves for porous beef-oil samples with and without support. It is observed that for all porosity values, the temperature difference is much smaller than that within beef-air samples. As with the beef-air samples, the temperature difference is largest for the sample with Alumina support on the right side. The temperature difference with Alumina support at the right side is around 53 K for $\phi = 0.6$ whereas it is around 36 K with no support. The temperature difference (ΔT_b) for Alumina support on the left side is around 29 K while for SiC support, the temperature difference is around 26 K at 80 s. The heating rates are shown via the inset plots and it is observed that the heating rates are not enhanced significantly in b/o samples with ceramic supports unlike the heating rates in b/a samples. The average temperature for $\phi = 0.6$ is around 340 K for SiC support, 340 K for Alumina support (right), 341 K for Alumina support (left) and 343 K for no support at 80 s.

3.3. Efficient heating strategies for beef-air and beef-oil systems: role of distributed microwave incidence

This section deals with microwave heating of b/a and b/o samples with different supports and with microwave incidence at both sides. As in the previous sections, the thickness of the support is assumed to be 0.2 cm for all the test cases. For both sides incidence, Alumina support is attached to the left side of the sample whereas SiC

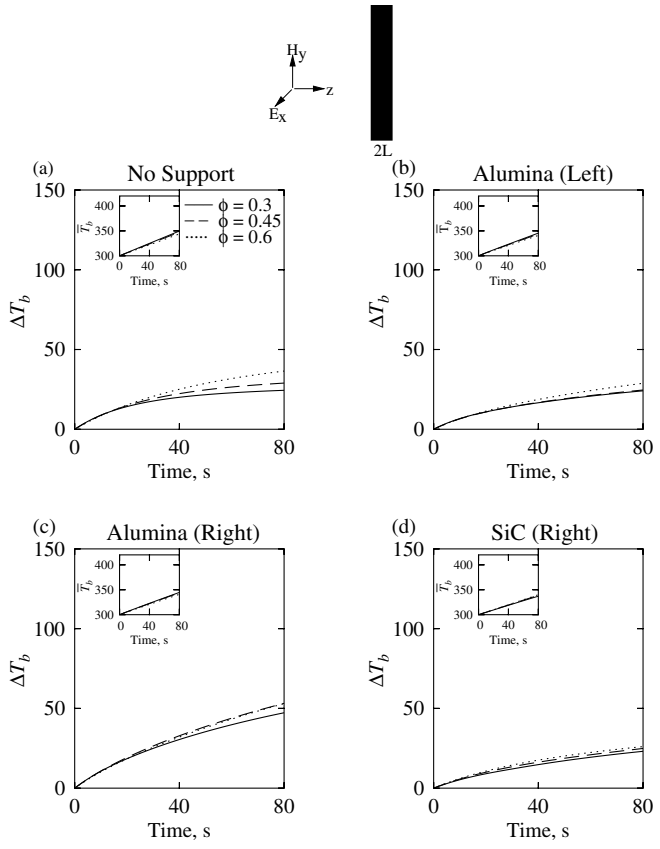

Fig. 10. The temperature difference, ΔT_b (K) vs time (s) for porous beef-oil samples ($\phi = 0.3$, 0.45 and 0.6) exposed to microwaves at one face during R_1 mode for (a) no support, (b) Alumina support at the left face, (c) Alumina support at the right face and (d) SiC support at the right face. The inset shows average temperature, $\overline{T}_b$ (K) vs time (s). Larger thermal runaway is observed for the samples with Alumina support at the right face. However, the degree of thermal runaway is smaller for b/o samples than that for b/a samples as seen in Fig. 7.

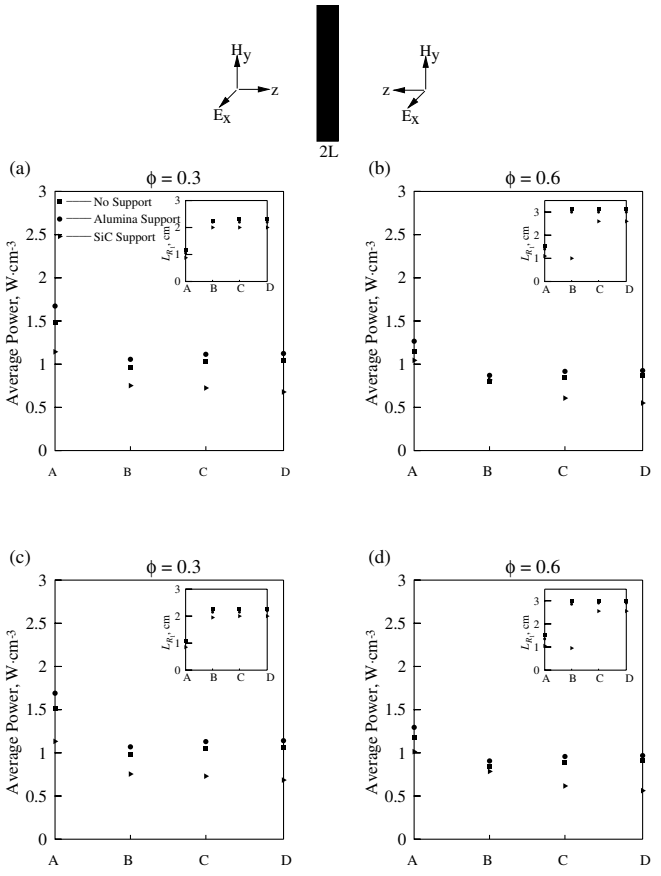

Fig. 11. Average power (W cm^{-3}) vs various distributions of microwave incidences (types A–D) for (a) beef-air sample with $\phi = 0.3$, (b) beef-air sample with $\phi = 0.6$, (c) beef-oil sample with $\phi = 0.3$ and (d) beef-oil sample with $\phi = 0.6$. The symbol, ■, denotes no support, the symbol, ●, denotes the Alumina support at the left face and the symbol, ▶, denotes SiC support at the right face. For all the cases, the type A distribution or one side incidence gives larger average power within the samples.

support is attached to the right face of the sample. For both sides incidence the total intensity of incident microwaves is maintained at 3 W cm^{-2}. Various combinations of microwave incidence at both sides are designated as A, B, C and D and the intensities at left and right sides are (3 and 0 W cm^{-2}), (2.5 and 0.5 W cm^{-2}), (2 and 1 W cm^{-2}) and (1.5 and 1.5 W cm^{-2}) for types A, B, C and D, respectively.

Fig. 11(a) and (b) show average power during R_1 mode for b/a samples vs types of microwave incidences for $\phi = 0.3$ and $\phi = 0.6$, respectively. It is observed that Alumina support shows larger average power within the sample with all types (A–D) of microwave incidences for $\phi = 0.3$ and 0.6 and the smallest power absorption within the sample occurs with SiC support. It is also observed that higher average power with and without supports are found for type A microwave incidence which corresponds to only one side incidence. The average power in the samples with type A incidence for no support, Alumina support and SiC support are 1.487, 1.673, and 1.144 W cm^{-3}, respectively corresponding to $\phi = 0.3$ (see Fig. 11(a)). The average power with and without support are smaller for type B, and the average power for types C and D incidences are of similar order of magnitudes for no support and ceramic support cases (see Fig. 11(a)). At $\phi = 0.6$, it is seen that almost identical average power is observed for types B–D incidences with Alumina support and without support (Fig. 11(b)). The insets show the sample thickness corresponding to R_1 mode (L_{R_1}) vs types of incidence. For $\phi = 0.3$, it is observed that higher sample thicknesses occur with types B–D microwave incidence with and without supports. For all types of incidence, SiC support corresponds to smaller sample thickness than those with Alumina support and no support. Similar behavior of sample thickness vs types of microwave incidence was observed for $\phi = 0.6$ with an exception of very small sample thickness with SiC support for type B incidence. In general, it is observed that average power absorption within the sample is smaller for $\phi = 0.6$ whereas the sample thickness is larger for $\phi = 0.6$ at specific types of incidence and support.

Fig. 11(c) and (d) show the average power distributions for b/o samples for $\phi = 0.3$ and 0.6. Variations in average power with type of incidence are similar to the identical

situation with b/a sample. For both b/a and b/o samples, it may be inferred that type A results in higher average power with and without support and for distributed microwave incidence, type D with identical intensities of microwave incidence at both sides results in higher average power. The efficiency of microwave heating with either one side incidence (type A) or with both sides incidence (type D) may also depend on spatial temperature distribution and thermal runaway situation which is examined next.

Fig. 12 shows the spatial distributions of electric fields, power and temperature for porous beef samples (b/a, $\phi = 0.6$) with and without support and with both sides incidence with equal intensities (type D). The distribution of microwave incidence reduces the average microwave power within the sample and it is seen that the average power varies between 0.55 and 0.93 W cm^{-3} with and without support. On the other hand, the average power varies between 1.04 and 1.26 W cm^{-3} for $\phi = 0.6$ with type A incidence. It is also seen that two spatial maxima in microwave power occur at both the faces with type A incidence whereas three maxima in spatial power occurs at the faces and the center with type D incidence except with SiC support. The distribution of microwave incidence plays an important role on spatial power absorption throughout the domain. It is further observed that the resultant stationary wave has a lower amplitude and therefore spatial power deposition is smaller than that in type A incidence. The support plays the role of altering the microwave power distribution and is similar to type A incidence. Alumina support enhances the microwave power within the sample. The spatial temperature distribution follows qualitatively the power distribution with no support and thermal runaway is observed at the center and both the faces with Alumina support and no support, respectively unlike type A incidence where thermal runaway occurs only near the faces. The thermal runaway with SiC support in presence of distributed microwave incidence is smaller than that with SiC support and type A incidence.

Fig. 13 shows the spatial distributions of electric fields, power and temperature for porous beef samples (b/o, $\phi = 0.6$) with and without support corresponding to both sides incidence with equal intensities (type D). As in the previous case for b/a sample, there are three local maxima in microwave power within the sample except for SiC support and the equi-distributed microwave power from both the faces reduce the microwave power distribution within the sample. The average power varies between 0.56 and 0.97 W cm^{-3}. Similar to microwave heating with type A incidence, the maxima in temperature is around 342 K for Alumina support and no support cases and the temperature is lower at the faces with SiC support. It is observed that the distribution of microwave incidence at both the sides do not alter significantly the thermal runaway within b/o samples with specific supports.

Fig. 14(a)–(c) show the temperature difference vs time plots for beef-air ($\phi = 0.6$) with and without support for the four types of incidence A, B, C and D. The inset shows average temperature vs time plots. For beef with no sup-

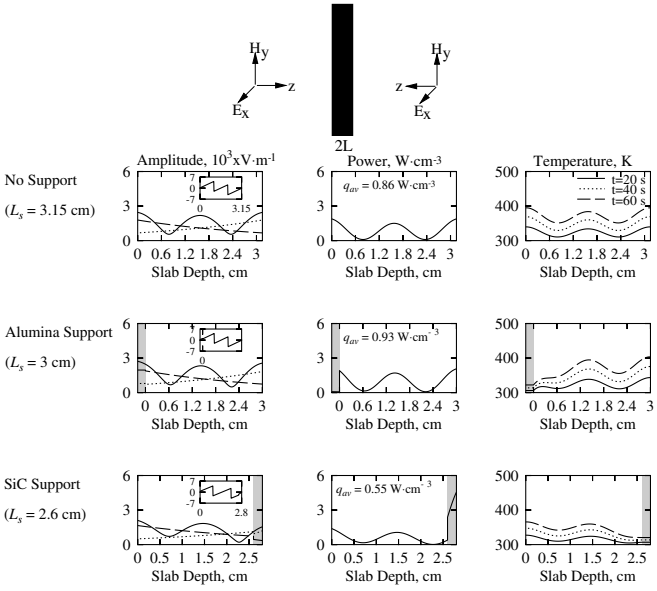

Fig. 12. Amplitudes of electric field $(A_{x,l}, A^{t}_{x,l}, A^{r}_{x,l})$, power distributions and temperature profiles for beef-air samples with type D or equi-distributed microwaves incidence for $\phi = 0.6$ with no support, Alumina support and SiC support cases during R_1 mode. The ceramic support thickness is 0.2 cm. (— —) Transmitted wave; (···) reflected wave; (——) stationary wave. The shaded regime denotes the ceramic support. The inset shows phase difference $(\delta_{x,l})$ vs z. Alumina support gives larger average power and high thermal runaway within the sample.

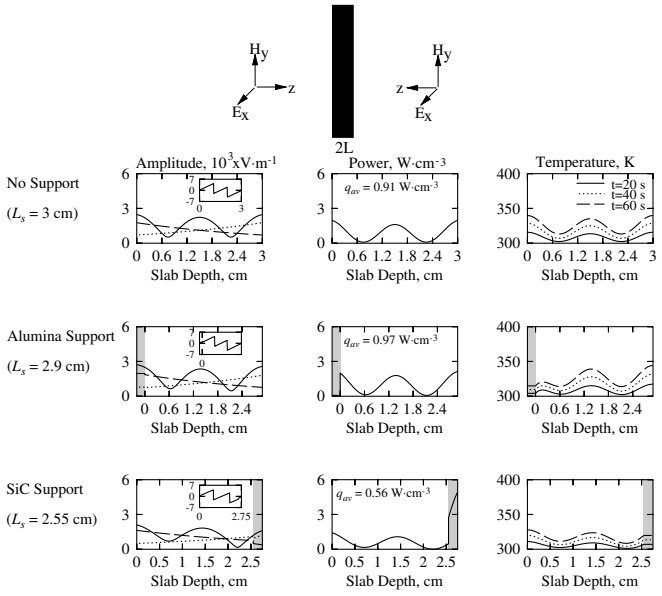

Fig. 13. Amplitudes of electric field $(A_{x,l}, A^{t}_{x,l}, A^{r}_{x,l})$, power distributions and temperature profiles for beef-oil samples with type D or equi-distributed microwaves incidence for $\phi = 0.6$ with no support, Alumina support and SiC support cases during R_1 mode. The ceramic support thickness is 0.2 cm. (— —) Transmitted wave; (···) reflected wave; (——) stationary wave. The shaded regime denotes the ceramic support. The inset shows phase difference $(\delta_{x,l})$ vs z. The thermal runaway is in general less for beef-oil samples.

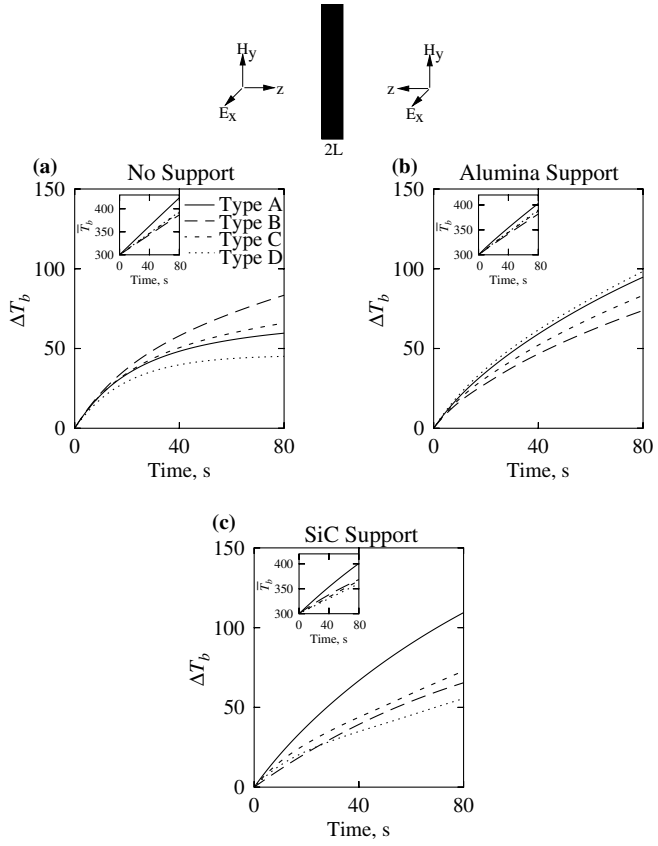

Fig. 14. The temperature difference, ΔT_b (K) vs time (s) for porous beef-air samples with $\phi = 0.6$ exposed to microwaves at both faces (types A–D) during R_1 mode for (a) no support, (b) Alumina support at the left face and (c) SiC support at the right face. The inset shows average temperature, $\overline{T}_b$ (K) vs time (s). The slope of average temperature vs time is higher for type A incidence with all cases. The thermal runaway is a strong function of various distributions of microwaves incidence for specific support assembly.

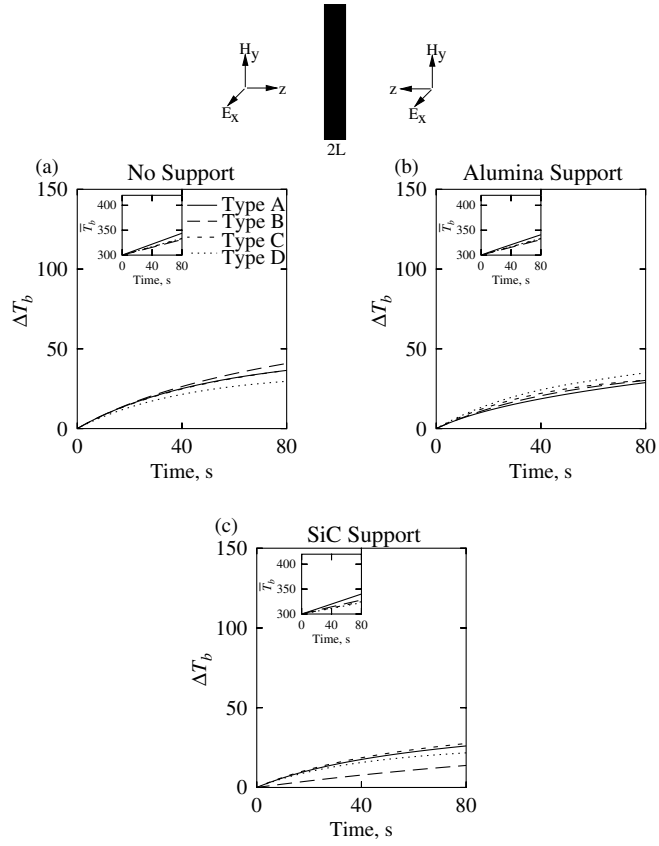

Fig. 15. The temperature difference, ΔT_b (K) vs time (s) for porous beef-oil samples with $\phi = 0.6$ exposed to microwaves at both faces (types A–D) during R_1 mode for (a) no support, (b) Alumina support at the left face and (c) SiC support at the right face. The inset shows average temperature, $\overline{T}_b$ (K) vs time (s). The slope of average temperature vs time is higher for type A incidence with all cases. Various distributions of microwave incidence do not have significant influence on the thermal runaway for specific support assembly.

port, it is observed that the temperature difference is highest with type B and lowest for type D at 80 s (Fig. 14(a)). The temperature difference is indicative of the degree of thermal runaway and it is observed that the thermal runaway is higher with types B and C whereas the lower thermal runaway is seen with one side incidence (type A) and equi-distributed both sides incidence (type D). The heating rate is quantified by the slope of average temperature vs time and type A gives higher heating rate. On the other hand, types A and D give rise to larger thermal runaway than types B and C for samples with Alumina support (Fig. 14(b)). For samples with SiC support, types B and D give lower thermal runaway (Fig. 14(c)). For all these cases, type A gives higher heating rates. The heating based on lower thermal runaway may occur with either equi-distributed or selectively distributed microwave incidence for beef-air (b/a) samples.

Fig. 15(a)–(c) show the temperature difference vs time plots for beef-oil ($\phi = 0.6$) with and without support for the four types of incidence A–D. The inset shows average temperature vs time plots. For no support, type D gives the lowest thermal runaway. For Alumina support cases, it is seen that the thermal runaway is generally small irrespective of the type of incidences (Fig. 15(a) and (b)) and for SiC support, type B incidence gives lower thermal runaway (Fig. 15(c)). For all the three cases, it is observed that type A incidence gives higher heating rates as can be seen from the inset plots. It may be noted that for b/o samples, selective types of incidence may reduce thermal runaway.

4. Conclusions

An extensive analysis on microwave heating of porous beef (beef-air and beef-oil) samples with and without ceramic supports and with different distributions of microwave incidence at both sides has been carried out. The average power within beef-air (b/a) and beef-oil (b/o) samples vs sample thicknesses for various porosities and with two resonance modes (R_1 and R_2) have been studied. Influence of various ceramic supports (Alumina and SiC) on average power distribution has been illustrated for three representative porosities ($\phi = 0.3$, 0.45 and 0.6). A mathematical

Table 2
The generalized heating strategies for beef-air (b/a) and beef-oil (b/o) samples

Heating strategy	Beef-air (b/a)	Beef-oil (b/o)
No Support	• Type A incidence gives largest heating rates • Types A and D incidences give lower thermal runaway • Types B–D incidences give larger processing thickness	• Type A incidence gives largest heating rates • Type D incidence gives lower thermal runaway • Types B–D incidences give larger processing thickness
Alumina Support	• Type A incidence gives largest heating rates • Types B and C incidences give lower thermal runaway • Types B–D incidences give larger processing thickness	• Type A incidence gives largest heating rates • Type A incidence gives smallest thermal runaway; types B–D also give small thermal runaway • Types B–D incidences give larger processing thickness
SiC Support	• Type A incidence gives largest heating rate • Types B and D incidences give lower thermal runaway • Types C and D incidences give larger processing thickness for higher porosity values	• Type A incidence gives largest heating rate • Type B incidence gives smallest thermal runaway • Types C and D incidences give largest processing thickness for higher porosity values

analysis has been carried out to study the role of individual traveling waves on spatial power and temperature distribution. It is observed that pure beef shows a higher average power than porous beef and that microwave power absorption decreases with increase in porosity at specific resonance modes (R_1 and R_2). For the beef-air (b/a) case, highest power is absorbed for the samples with Alumina support attached at the left face and lowest power with SiC support on right face with one side incidence. For beef-oil (b/o) cases, the supports have a smaller influence on the power absorbed within the sample. Finally, an efficient heating strategy has been described with temperature difference (ΔT_b) and average temperature ($\overline{T_b}$) vs time plot in presence of various distributed microwave incidences. The heating rate may be quantified by the slope of average temperature vs time plot and thermal runaway is measured with the distribution of temperature difference. In general, it is observed that the higher thermal runaway is observed for $\phi = 0.6$ with b/a samples whereas the thermal runaway is lower and almost independent of porosity for b/o samples.

Table 2 shows the heating characteristics for various heating strategies such as with no support, Alumina support and SiC support. Choice of suitable distributions of microwave incidences is a strong function of heating with various supports or without supports. The distributed heating or one side heating is preferred based on maxima in heating rates with smaller thermal runaway.

It is observed that for no-support case with b/a samples, types A and D incidences may be the optimal choices of heating with smaller thermal runaway. In contrast, types B and D incidences correspond to smaller thermal runaway for heating b/a samples with Alumina and SiC supports. It may be noted that, type A or one side heating gives the largest heating rates for all the heating strategies with and without support cases. The distributed heating with type B, C or D may give larger processing thickness. Therefore optimal and efficient processing of b/a samples would depend on four factors such as heating rates, thermal runaway, processing thickness and porosities.

It is observed that b/o sample with Alumina support may be optimally heated with type A incidence as it corresponds to largest heating rates with smaller thermal runaway. Here, Alumina support with type A incidence refers to the sample with support at the left face. For no support and SiC support cases, type A may give largest heating rates; however type B or D incidence gives smaller thermal runaway. As in b/a sample, the larger processing thickness is also obtained with type B, C or D incidence.

It is seen that the distributed microwave sources at both the sides may reduce the runaway heating effects for certain cases. The heating characteristics as seen in Table 2 may be useful to provide a guideline for optimal microwave processing of porous materials with/without different ceramic supports.

References

[1] K.G. Ayappa, H.T. Davis, E.A. Davis, J. Gordon, Analysis of microwave heating of materials with temperature-dependent properties, Am. Inst. Chem. Eng. J. 37 (1991) 313–322.
[2] K.G. Ayappa, H.T. Davis, E.A. Davis, J. Gordon, Two-dimensional finite element analysis of microwave heating, Am. Inst. Chem. Eng. J. 38 (1992) 1577–1592.
[3] S.A. Barringer, E.A. Davis, J. Gordon, K.G. Ayappa, H.T. Davis, Effect of sample size on microwave heating rate: oil vs water, Am. Inst. Chem. Eng. J. 40 (1994) 1433–1439.
[4] K.G. Ayappa, H.T. Davis, S.A. Barringer, E.A. Davis, Resonant microwave power absorption in slabs and cylinders, Am. Inst. Chem. Eng. J. 43 (1997) 615–624.
[5] T. Basak, K.G. Ayappa, Influence of internal convection during microwave thawing of cylinders, Am. Inst. Chem. Eng. J. 47 (2001) 835–850.
[6] T. Basak, K.G. Ayappa, Role of length scales on microwave thawing dynamics in 2D cylinders, Int. J. Heat Mass Transfer 45 (2002) 4543–4559.
[7] T. Basak, Analysis of resonances during microwave thawing of slabs, Int. J. Heat Mass Transfer 46 (2003) 4279–4301.
[8] T. Basak, Role of resonances on microwave heating of oil–water emulsions, Am. Inst. Chem. Eng. J. 50 (2004) 2659–2675.
[9] T. Basak, Analysis of microwave propagation for multilayered material processing: Lambert's law versus exact solution, Indust. Eng. Chem. Res. 43 (2004) 7671–7675.
[10] T. Basak, A.S. Priya, Role of ceramic supports on microwave heating of materials, J. Appl. Phys. 97 (2005). Art. No. 083537.
[11] T. Basak, A.S. Priya, Role of metallic and ceramic supports on enhanced microwave heating processes, Chem. Eng. Sci. 60 (2005) 2661–2677.
[12] G.H. Chen, W. Wang, A.S. Mujumdar, Theoretical study of microwave heating patterns on batch fluidized bed drying of porous material, Chem. Eng. Sci. 56 (2001) 6823–6835.

[13] P. Ratanadecho, K. Aoki, M. Akahori, Influence of irradiation time, particle sizes, and initial moisture content during microwave drying of multi-layered capillary porous materials, J. Heat Transfer Trans. ASME 124 (2002) 151–161.
[14] H.W. Wu, Z. Tao, G.H. Chen, H.W. Deng, G.Q. Xu, S.T. Ding, Conjugate heat and mass transfer process within porous media with dielectric cores in microwave freeze drying, Chem. Eng. Sci. 59 (2004) 2921–2928.
[15] D.D. Dincov, K.A. Parrott, K.A. Pericleous, Heat and mass transfer in two-phase porous materials under intensive microwave heating, J. Food Eng. 65 (2004) 403–412.
[16] P. Salagnac, P. Glouannec, D. Lecharpentier, Numerical modeling of heat and mass transfer in porous medium during combined hot air, infrared and microwaves drying, Int. J. Heat Mass Transfer 47 (2004) 4479–4489.
[17] H. Fricke, The complex conductivity of a suspension of stratified particles of spherical or cylindrical form, J. Phys. Chem. 59 (1955) 168–174.
[18] A. Chatterjee, T. Basak, K.G. Ayappa, Analysis of microwave sintering of ceramics, Am. Inst. Chem. Eng. J. 44 (1998) 2302–2311.
[19] J.N. Reddy, An Introduction to the Finite Element Method, McGraw-Hill, New York, 1993.